photonics

MDPI

Article

Optical Angular Momentum Beam Generation Using Coherent Beam Combination

Przemyslaw Gontar, Lukasz Gorajek, Waldemar Zendzian and Jan Jabczyński *

Institute of Optoelectronics, Military University of Technology, ul. gen. S. Kaliskiego 2, 00-908 Warsaw, Poland; przemyslaw.gontar@wat.edu.pl (P.G.); lukasz.gorajek@wat.edu.pl (L.G.); waldemar.zendzian@wat.edu.pl (W.Z.)
* Correspondence: jan.jabczynski@wat.edu.pl; Tel.: +48-261-839-617

Abstract: (1) Background: The significant progress observed over the last two decades in coherent beam combining (CBC) technology has mainly focused on its applications in high-energy physics and laser weapons. This work provides insight into the basic principles of CBC and the search for an alternative, namely optical angular momentum (OAM) generation using CBC. (2) Methods: A semi-analytical model based on the paraxial wave equation was explored, generating OAM-CBC beams by manipulating the tilts and phases of the CBC (T&P-CBC) of hexagonal architecture. (3) Results: The specially arranged T&P-CBC shows typical properties of OAM, such as annular profiles for the zero diffraction order and 1st-order replicas in the far field and correlation coefficients of 1% between different OAM-CBC fields. (4) Conclusions: The differences between classical OAM beams and OAM-CBC are substantial due to hexagonal lattice properties. Moreover, applications in free space optical communications are feasible as T&P CBC fulfills the main conditions and requirements for OAM generation.

Keywords: laser beams; coherent beam combining; optical angular momentum; vortex beams; free-space optical communications

Citation: Gontar, P.; Gorajek, L.; Zendzian, W.; Jabczyński, J. Optical Angular Momentum Beam Generation Using Coherent Beam Combination. *Photonics* **2024**, *11*, 907. https://doi.org/10.3390/photonics11100907

Received: 20 August 2024
Revised: 23 September 2024
Accepted: 25 September 2024
Published: 26 September 2024

1. Introduction

Coherent beam combination (CBC) technology, including filled aperture CBC (FA-CBC) and tiled aperture CBC (TA-CBC) [1–11], has been developed in the last two decades, mainly for applications in laser weapons [4,12] and high-energy physics [6,10]. FA-CBC offers high efficiency and robustness, but it is limited by the number of emitters (not higher than 12 beams for a high-average-power system [13]). In contrast, TA-CBC offers direct scalability beyond hundreds of combined beams, but has low practical efficiency [5,10,11] and difficulty scaling to high average powers. Both technologies require effective adaptive optics subsystems for outdoor applications, such as laser weapons and free-space optical communications (FSOC), over long propagation distances in horizontal directions [8,9,14,15] and/or in Earth–satellite FSOC links [16–18].

Since the 1990s, optical angular momentum (OAM) beams have been examined theoretically and experimentally, attracting [19–23] growing interest in material processing, optical tweezing and FSOC [16,18,23–28]. The benefits of OAM technology include propagation invariance as 'diffraction-free' solutions of paraxial wave equations, enhanced resilience to atmospheric turbulence and orthogonality, enabling potential increases in FSOC channel bandwidth thanks to spatial multiplexing. However, its scalability in power and practical realization in laboratory and outdoor applications are problematic for a single-aperture output.

The purpose of this study was to merge both technologies, that is, to search for the possibilities of CBC technology for the generation of OAM beams (OAM-CBC). Preliminary results were presented in [29], where a segmented vortex wavefront was constructed in the near field owing to a special helix-like stepped phase shift in the hexagonal lattice. Here, we

develop this approach for a special tilted and phased CBC (T&P-CBC) concept, enabling the effective construction of segmented vortex wavefronts in the near field. Section 2 describes the semi-analytical model of CBC propagation and the OAM-CBC concept. The main results, analysis, and discussion are presented in Section 3, and conclusions are drawn in Section 4.

2. Tilted and Phased CBC for Optical Angular Momentum Generation

Here, we give only a brief description of the analysis method. The full mathematical model is described in detail in [30,31]. To start, we provide the main characteristics of CBC hexagonal architecture (see Figure 1). The center and chief ray directions of each (l, n)-th emitter/beam of the CBC are defined by the geometry of the hexagonal lattice; N_{cr} is the number of crowns; $N_{lat} = 3N_{cr}\,(N_{cr} + 1) + 1$ is the number of emitters; a is the half period of the lattice; r_a is the sub-aperture radius; $f.f. = r_a/a$ is the filling factor; and f is the focal length. In the classical CBC configuration, each chief ray is directed to the common focal point F, with a spherical segmented wavefront of the CBC lattice of the radius f. The diffraction profiles of CBC in the far field are characterized by the Airy radius $r_{Airy} = 0.61\lambda/NA_{lat}$ and Fresnel range $Z_{Fresnel} = \lambda/NA_{lat}{}^2$, where $NA_{lat} = (N_{cr} + 1/2)2a/f.$ is the numerical aperture of the lattice and λ is the wavelength.

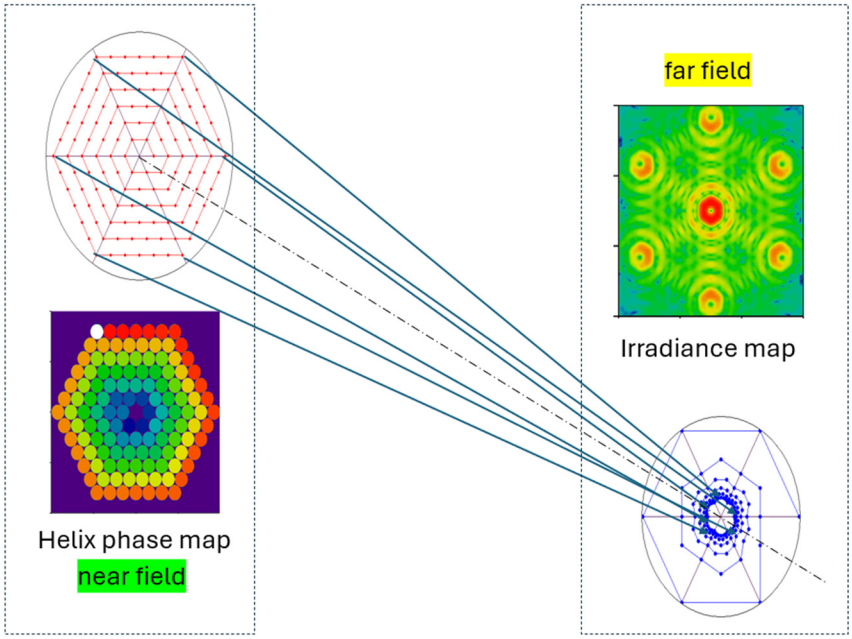

Figure 1. Concept of optical angular momentum–coherent beam combining (OAM-CBC) generation via tilted and phased CBC.

We applied a truncated Gaussian beam as a 'prototype' optical field. To simplify calculations, we used the once-determined and calculated approximate solution of a truncated Gaussian beam for the given beam radius w_1 at the aperture and truncation level $\varepsilon_{\mathrm{tr}} = \exp(-2(r_a/w_1)^2)$ (see [32]), which is valid over a wide range of propagation distances in the vicinity of focal point F. Note that the ratio of the Rayleigh range of an individual beam to the caustics length defined by the Fresnel range is proportional to $N_{cr}{}^2$. Typically, for long-distance propagation, the Rayleigh range is comparable to f ('collimation case'), whereas the Fresnel range is N_{lat} times shorter. We calculated the coherent sum of all input beams for the specific distribution of phases and tilts for a chosen plane near focal point F.

Evidently, various T&P-CBC realizations exist in the $(1 + 3) \times N_{lat}$ dimensional space of the control parameters. The exploration of this subject is far beyond the scope of this study. Here, we focus on the OAM-CBC case. We define a specific segmented vortex wavefront with a step-like helix phase and tilt vector $[\theta_x, \theta_y]$ in the near field as follows:

The OAM-CBC amplitude $B_{m_{\mathrm{OAM}}}$ with the given m_{OAM}—optical angular momentum number can be described as follows:

$$B_{m_{\mathrm{OAM}}} = \sum_{l,n} A_{l,n} \exp[ik\Phi_{l,n}] \text{ where } \Phi_{l,n} = \frac{{r_{l,n}}^2}{f} + m_{\mathrm{OAM}} \frac{\varphi_{l,n}}{k} \quad (1)$$

Here, l and n are the indices of the sub-aperture, $A_{l,n}$ is the amplitude of the (l, n) sub-aperture, $r_{l,n}$ and $\varphi_{l,n}$ are the radius to the lattice center and the azimuth angle of each sub-aperture, f is the focal length, and k is the wavenumber.

Next, we the calculate vortex tilt vector $[\theta_x, \theta_y]$ by the gradient $\nabla\Phi_{l,n}$ as follows:

$$\nabla\Phi_{l,n} = \left[\theta_{x,l,n}\ ,\ \theta_{y,l,n}\right] = \left[\frac{r_{l,n}\cos\varphi_{l,n}}{f} + m_{\mathrm{OAM}}\frac{\sin\varphi_{l,n}}{kr_{l,n}}\ ,\quad \frac{r_{l,n}\sin\varphi_{l,n}}{f} - m_{\mathrm{OAM}}\frac{\cos\varphi_{l,n}}{kr_{l,n}}\right] \quad (2)$$

Note that for $m_{\mathrm{OAM}} \neq 0$, the geometrical-optics caustics of the OAM-CBC vortex segmented wavefront has a coiling non-linear helix shape with an inner hole (lower right part of Figure 1) corresponding to the evolving hexagonal helix of the CBC in the near field (upper left part in Figure 1). The coiling helix for $m_{\mathrm{OAM}} = 0$ transforms into a distinct focal point F for the classical spherical CBC case. This phenomenon is a direct geometrical-optics interpretation of vanishing irradiance at $r = 0$ and an annular amplitude distribution in caustics for the vortex OAM beam.

3. Results

We tested the proposed OAM-CBC concept for a large hexagonal lattice consisting of $N_{cr} = 6$ outer crowns ($N_{lat} = 127$ emitters), assuming very dense packing (*f.f.* = 0.99). To neglect the peculiarities of diffraction, we assumed low truncation losses $\varepsilon_{\mathrm{tr}} = 0.05$. Thus, an 'almost' Gaussian beam was emitted by an individual emitter with a very low power content at higher diffraction orders in the caustics region. The hexagonal architecture of the CBC reflects the six-folded symmetry of the 1st diffraction orders (see Figure 2).

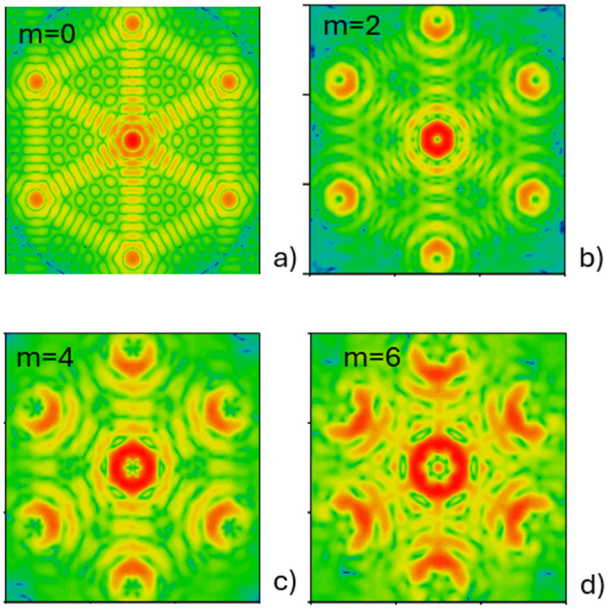

Figure 2. Two-dimensional maps of OAM-CBC irradiance distributions (in logarithmic scale) in the far field for optical angular momentum number; (**a**) $m_{\mathrm{OAM}} = 0$; (**b**) 2; (**c**) 4; (**d**) 6; $N_{lat} = 127$, *f.f.* = 0.99, $\varepsilon_{\mathrm{tr}} = 0.05$.

The basic compliance between the geometrical-optics caustics (Figure 1) and wave optics demonstrate a dominant annular profile in the zero-order diffraction area (Figures 2–4). In Figure 2, the irradiance maps for $m_{\mathrm{OAM}} > 0$ (Figure 2b–d) exhibit the expected properties

of the conjunction of CBC and OAM beams. The zero-diffraction order has a nearly annular shape and the 1st diffraction orders resemble its replicas.

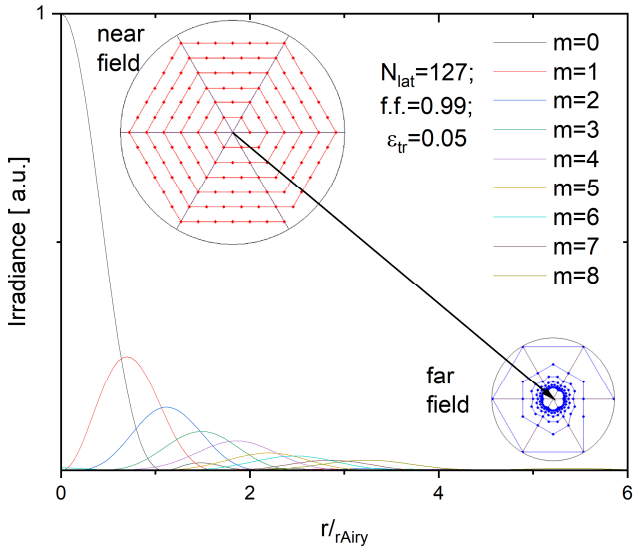

Figure 3. Irradiance profiles in the far field for m_{OAM} ϵ [0, 8]; *f.f.* = 0.99, $\varepsilon_{\mathrm{tr}}$ = 0.05, N_{lat} = 127.

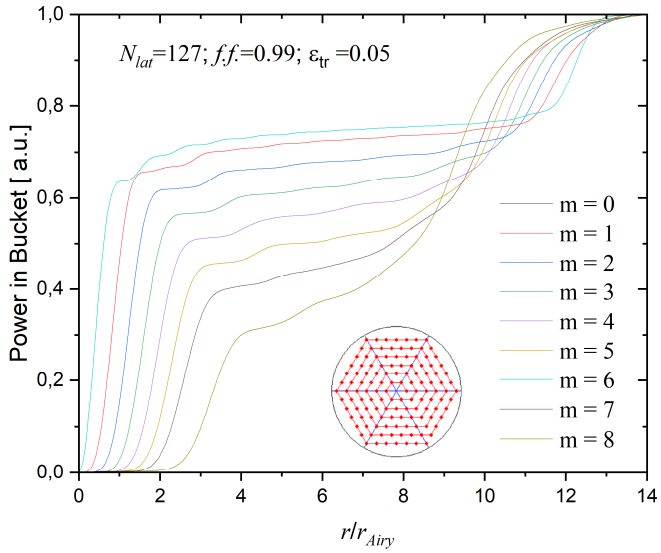

Figure 4. Power-in-bucket curves for m_{OAM} ϵ [0, 8]; *f.f.* = 0.99, $\varepsilon_{\mathrm{tr}}$ = 0.05, N_{lat} = 127.

The typical dependencies of the far field profiles and power-in-bucket (PIB) curves for OAM-CBC are shown in Figures 3 and 4.

With an increase in m_{OAM}, the amplitude profiles worsen with flattening and dissipation of power density out of the low diffraction lobes (Figures 3 and 4). Moreover, above $m_{\mathrm{OAM}} > 5$, the 2D maps resemble the aberrated and scattered partly coherent beams with the minimum at the axis. These features are particularly highlighted for $m_{\mathrm{OAM}} = 6$ (Figure 2d), for which the six-fold symmetries of the vortex and hexagonal lattice overlap.

To examine the orthogonality of a set of OAM-CBC amplitude profiles in the far field and their feasibility in FSOC, we calculated the correlation coefficients $\gamma_{m,k}$ defined as follows:

$$\gamma_{m,k} = \frac{\langle B_m {B_k}^* \rangle}{\sqrt{\langle B_m {B_m}^* \rangle \langle B_k {B_k}^* \rangle}} \tag{3}$$

where $\langle B_m {B_k}^* \rangle$ denotes the discrete 2D summation of $B_m {B_k}^*$ over a finite area in the far field; (15 × 15 r_{Airy} in our case).

The results of the $\gamma_{m,k}$ calculations for a trail of nine configurations with $m_{\mathrm{OAM}} \in [0, 8]$ are collected in Table 1.

Table 1. Correlation coefficients for OAM-CBC amplitude profiles in the far field; $m_{\mathrm{OAM}} \in [0, 8]$, *f.f.* = 0.99, $\varepsilon_{\mathrm{tr}} = 0.05$, $N_{lat} = 127$.

m_{OAM}	**0**	**1**	**2**	**3**	**4**	**5**	**6**	**7**	**8**
0	1.00000	0.00844	0.00875	0.00924	0.00986	0.01000	**0.10100**	0.01200	0.01200
1	0.00844	1.00000	**0.00484**	0.00507	0.00541	0.00570	0.00848	0.08800	0.00701
2	0.00875	0.00484	1.00000	0.00530	0.00562	0.00599	0.00862	0.00681	0.09500
3	0.00924	0.00507	0.00530	1.00000	0.00592	0.00621	0.00918	0.00770	0.00768
4	0.00986	0.00541	0.00562	0.00592	1.00000	0.00669	0.00958	0.00761	0.00843
5	0.01000	0.00570	0.00599	0.00621	0.00669	1.00000	0.01000	0.00846	0.00868
6	0.10100	0.00848	0.00862	0.00918	0.00958	0.01000	1.00000	0.01100	0.01200
7	0.01200	0.08800	0.00681	0.00770	0.00761	0.00846	0.01100	1.00000	0.00987
8	0.01200	0.00701	0.09500	0.00768	0.00843	0.00868	0.01200	0.00987	1.00000

Nonperfect orthogonality is caused by the characteristics of the OAM-CBC concept (discrete 2D array of hexagonal symmetry), numerical errors, the approximate solution of the truncated Gaussian beam, and discrete summation over a limited area.

The values of $\gamma_{m,k}$ were in the range [0.0048, 0.1]. For a narrow range of $m_{\mathrm{OAM}} \in [0, 5]$ the average correlation coefficient $\gamma_{m,k} = 0.7\%$, whereas for a $m_{\mathrm{OAM}} \in [0, 8]$ it increases to 1.5%. We suppose that a correlation coefficient of 1%, corresponding to the cross-channel crosstalk, is acceptable for practical applications in FSOC. Thus, we can conclude that the T&P-CBC sufficiently satisfies the main conditions and requirements of OAM generation.

4. Conclusions

Our numerical experiments demonstrated the feasibility of the merging of OAM and CBC technologies. For a densely packed CBC hexagonal array, the vortex wavefront was emulated with a step-like evolving helix of phase and tilt vectors in the near field.

i/ The irradiance maps for $m_{\mathrm{OAM}} > 0$ exhibit the expected properties of a combination of CBC and OAM beams. The zero-diffraction order has a nearly annular shape and the 1st diffraction orders resemble its replicas. However, the differences between classical OAM beams and OAM-CBC are substantial owing to their hexagonal lattice properties.

ii/ The imperfect orthogonality of the OAM-CBC set is attributed to the specific characteristics of the OAM-CBC concept (discrete 2D array of hexagonal symmetry), numerical errors and discrete summation over a limited area. For the m_{OAM} range of [0, 5], the average correlation coefficient, corresponding to cross-channel crosstalk, is 0.7%, which is acceptable for practical applications in FSOC.

We conclude that the proposed T&P-CBC concept fulfills the primary conditions and requirements for OAM generation. In further research, we intend to examine the rules of OAM-CBC algebra and the impact of lattice architecture parameters and imperfections.

Author Contributions: Conceptualization, J.J. and W.Z.; methodology, L.G., W.Z. and J.J.; software, P.G. and L.G.; data curation, P.G.; writing—J.J.; writing—review and editing, P.G. and J.J.; visualization, P.G.; supervision, J.J. All authors have read and agreed to the published version of the manuscript.

Funding: This research received no external funding.

Institutional Review Board Statement: Not applicable.

Informed Consent Statement: Not applicable.

Data Availability Statement: The dataset is available on request from the authors.

Acknowledgments: We would like to express our gratitude to Janusz Mikołajczyk and Aluś Emo Capodilista for their helpful support and discussion.

Conflicts of Interest: The authors declare no conflicts of interest.

References

1. Brignon, A. *Coherent Laser Beam Combining*, 2013th ed.; Brignon, A., Ed.; Wiley-VCH, Verlag GmbH & Co. KGaA: Weinheim, Germany, 2013; ISBN 978-3-527-65280-8.
2. Fathi, H.; Närhi, M.; Gumenyuk, R. Towards Ultimate High-Power Scaling: Coherent Beam Combining of Fiber Lasers. *Photonics* **2021**, *8*, 566. [CrossRef]
3. Fan, T.Y. Laser Beam Combining for High-Power, High-Radiance Sources. *IEEE J. Sel. Top. Quantum Electron.* **2005**, *11*, 567–577. [CrossRef]
4. Van Zandt, N.R.; Cusumano, S.J.; Bartell, R.J.; Basu, S.; McCrae, J.E.; Fiorino, S.T. Comparison of Coherent and Incoherent Laser Beam Combination for Tactical Engagements. *Opt. Eng.* **2012**, *51*, 104301. [CrossRef]
5. Shpakovych, M.; Maulion, G.; Kermene, V.; Boju, A.; Armand, P.; Desfarges-Berthelemot, A.; Barthélemy, A. Experimental Phase Control of a 100 Laser Beam Array with Quasi-Reinforcement Learning of a Neural Network in an Error Reduction Loop. *Opt. Express* **2021**, *29*, 12307. [CrossRef]
6. Mourou, G.; Brocklesby, B.; Tajima, T.; Limpert, J. The Future Is Fibre Accelerators. *Nat. Photonics* **2013**, *7*, 258–261. [CrossRef]
7. Leshchenko, V.E. Coherent Combining Efficiency in Tiled and Filled Aperture Approaches. *Opt. Express* **2015**, *23*, 15944. [CrossRef] [PubMed]
8. Jabczyński, J.K.; Gontar, P. Impact of Atmospheric Turbulence on Coherent Beam Combining for Laser Weapon Systems. *Def. Technol.* **2021**, *17*, 1160–1167. [CrossRef]
9. Weyrauch, T.; Vorontsov, M.; Mangano, J.; Ovchinnikov, V.; Bricker, D.; Polnau, E.; Rostov, A. Deep Turbulence Effects Mitigation with Coherent Combining of 21 Laser Beams over 7 Km. *Opt. Lett.* **2016**, *41*, 840. [CrossRef]
10. Fsaifes, I.; Daniault, L.; Bellanger, S.; Veinhard, M.; Bourderionnet, J.; Larat, C.; Lallier, E.; Durand, E.; Brignon, A.; Chanteloup, J.-C. Coherent Beam Combining of 61 Femtosecond Fiber Amplifiers. *Opt. Express* **2020**, *28*, 20152. [CrossRef]
11. Chang, H.; Chang, Q.; Xi, J.; Hou, T.; Su, R.; Ma, P.; Wu, J.; Li, C.; Jiang, M.; Ma, Y.; et al. First Experimental Demonstration of Coherent Beam Combining of More than 100 Beams. *Photonics Res.* **2020**, *8*, 1943. [CrossRef]
12. Sprangle, P.; Ting, A.; Peñano, J.; Fischer, R.; Hafizi, B. Incoherent Combining and Atmospheric Propagation of High-Power Fiber Lasers for Directed-Energy Applications. *IEEE J. Quantum Electron.* **2009**, *45*, 138–148. [CrossRef]
13. Müller, M.; Aleshire, C.; Klenke, A.; Haddad, E.; Légaré, F.; Tünnermann, A.; Limpert, J. 10.4 KW Coherently Combined Ultrafast Fiber Laser. *Opt. Lett.* **2020**, *45*, 3083. [CrossRef] [PubMed]
14. Vorontsov, M.; Filimonov, G.; Ovchinnikov, V.; Polnau, E.; Lachinova, S.; Weyrauch, T.; Mangano, J. Comparative Efficiency Analysis of Fiber-Array and Conventional Beam Director Systems in Volume Turbulence. *Appl. Opt.* **2016**, *55*, 4170. [CrossRef] [PubMed]
15. Weyrauch, T.; Vorontsov, M.A.; Carhart, G.W.; Beresnev, L.A.; Rostov, A.P.; Polnau, E.E.; Liu, J.J. Experimental Demonstration of Coherent Beam Combining over a 7 km Propagation Path. *Opt. Lett.* **2011**, *36*, 4455–4457. [CrossRef] [PubMed]
16. Meric, H. Atmospheric Turbulence Modeling and Aperture Analysis for Optimizing Receiver Design and System Performance on Free Space Optical Communication Links. Master's Thesis, Bilkent Universitesi, Ankara, Türkiye, 2012.
17. Andrews, L.C.; Phillips, R.L. *Laser Beam Propagation through Random Media*; SPIE: Bellingham, WA, USA, 2005; ISBN 0-8194-5948-8.
18. Stotts, L.B.; Andrews, L.C. Optical Communications in Turbulence: A Tutorial. *Opt. Eng.* **2023**, *63*, 041207. [CrossRef]
19. Allen, L.; Barnett, S.M.; Padgett, M.J. *Optical Angular Momentum*; CRC Press: Boca Raton, FL, USA, 2016; ISBN 9781482269017.
20. Lian, Y.; Qi, X.; Wang, Y.; Bai, Z.; Wang, Y.; Lu, Z. OAM Beam Generation in Space and Its Applications: A Review. *Opt. Lasers Eng.* **2022**, *151*, 106923. [CrossRef]
21. Shiri, A.; Gbur, G. Orbital Angular Momentum Spectrum of Model Partially Coherent Beams in Turbulence. *Opt. Express* **2024**, *32*, 18175. [CrossRef] [PubMed]
22. Hou, T.; Zhang, Y.; Chang, Q.; Ma, P.; Su, R.; Wu, J.; Ma, Y.; Zhou, P. High-Power Vortex Beam Generation Enabled by a Phased Beam Array Fed at the Nonfocal-Plane. *Opt. Express* **2019**, *27*, 4046. [CrossRef]
23. Yu, T.; Xia, H.; Xie, W.; Peng, Y. Orbital Angular Momentum Mode Detection of the Combined Vortex Beam Generated by Coherent Combining Technology. *Opt. Express* **2020**, *28*, 35795. [CrossRef] [PubMed]
24. Vetter, C.; Steinkopf, R.; Bergner, K.; Ornigotti, M.; Nolte, S.; Gross, H.; Szameit, A. Realization of Free-Space Long-Distance Self-Healing Bessel Beams. *Laser Photonics Rev.* **2019**, *13*, 1900103. [CrossRef]
25. Rouzé, B.; Lombard, L.; Jacqmin, H.; Liméry, A.; Durécu, A.; Bourdon, P. Coherent Beam Combination of Seven 1.5 Mm Fiber Amplifiers through up to 1 Km Atmospheric Turbulence: Near- and Far-Field Experimental Analysis. *Appl. Opt.* **2021**, *60*, 8524. [CrossRef] [PubMed]
26. Doster, T.; Watnik, A.T. Laguerre–Gauss and Bessel–Gauss Beams Propagation through Turbulence: Analysis of Channel Efficiency. *Appl. Opt.* **2016**, *55*, 10239. [CrossRef] [PubMed]

27. Fiorino, S.T.; Bartell, R.J.; Krizo, M.J.; Caylor, G.L.; Moore, K.P.; Harris, T.R.; Cusumano, S.J. A First Principles Atmospheric Propagation & Characterization Tool: The Laser Environmental Effects Definition and Reference (LEEDR). In *Atmospheric Propagation of Electromagnetic Waves II*; SPIE: Bellingham, WA, USA, 2008; Volume 6878, pp. 57–68.
28. Aksenov, V.P.; Dudorov, V.V.; Filimonov, G.A.; Kolosov, V.V.; Venediktov, V.Y. Vortex Beams with Zero Orbital Angular Momentum and Non-Zero Topological Charge. *Opt. Laser Technol.* **2018**, *104*, 159–163. [CrossRef]
29. Jabczynski, J.K.; Gontar, P.; Gorajek, L.; Zendzian, W. Segmented Vortex Wavefront Coherent Beam Combining. *AIP Adv.* **2022**, *12*, 045223. [CrossRef]
30. Jabczynski, J.K.; Gontar, P. Analysis of the Caustics of Partially Coherently Combined Truncated Gaussian Beams. *Appl. Opt.* **2020**, *59*, 3340. [CrossRef]
31. Jabczyński, J.K.; Gontar, P.; Gorajek, Ł.; Żendzian, W. Simplified Sensitivity Analysis of Coherent Beam Combining in a Tiled Aperture Architecture. *Appl. Opt.* **2021**, *60*, 5012–5019. [CrossRef] [PubMed]
32. Ding, D.; Liu, X. Approximate Description for Bessel, Bessel-Gauss, and Gaussian Beams with Finite Aperture. *JOSA A* **1999**, *16*, 1286–1293. [CrossRef]